

Transactions on
Computational Modeling and Intelligent Systems

Volume 4, July 2026, Article 10087
https://doi.org/10.65112.tcmis.10087

eISSN: 3108-5202
www.tcmis.org

RESEARCH ARTICLE

Nonlinear buoyancy-driven thermal energy transport on a moving vertical plate with boundary slips and non-uniform heat source/sink

Astick Banerjee[1], Sohita Rajput[2*], Krishnendu Bhattacharyya[3], Mitu Dular[3], Dimpal Sharma[3] and Sanat Kumar Mahato[4]

[1]*Department of Mathematics and Computing, Biswa Bangla Biswabidyalay, Bolpur, Birbhum-723104, West Bengal, India.*
[2]*Mathematics Section, Department of Science and Humanity, Sershah Engineering College, Sasaram-821113, Bihar, India.*
[3]*Department of Mathematics, Institute of Science, Banaras Hindu University, Varanasi-221005, Uttar Pradesh, India.*
[4]*Department of Mathematics, Sidho-Kanho-Birsha University, Purulia-723104, West Bengal, India.*

[*]*Corresponding Author. Email: sohita.math@gmail.com (S. Rajput)*

Article Information

Received: 17 May 2026
Accepted: 15 July 2026
Published: 19 July 2026

AMS 2020 Classification:
76D10, 80A19

Abstract

This work investigates the key controlling mechanisms of two-dimensional buoyancy-driven nonlinear mixed convection and thermal energy transport in the flow generated by a vertically moving plate with partial slip and variable heat source/sink effects. The problem is motivated by applications in nuclear power systems, polymer processing, and other industrial operations where nonlinear heat convection and controllable heat generation are essential. By employing suitable similarity transformations, the governing nonlinear partial differential equations are reduced to coupled ordinary differential equations, which are solved using the MATLAB bvp4c solver. A combination of graphical and tabulated results is used to illustrate the influence of key controlling parameters. The analysis uncovers several notable physical trends. Nonlinear mixed convection significantly lowers fluid temperature while enhancing near-wall velocity. Both temperature-dependent and space-dependent heat sources or sinks intensify or reduce the velocity and temperature distributions and simultaneously cause the thickening or thinning of the associated boundary layers. Velocity slip and thermal jump at the surface reduce the near-wall momentum, which causes a reduction in velocity inside the boundary layer. Heat sources, whether spatially-dependent or temperature-dependent, consistently reduce surface drag force and cooling rate, whereas heat sinks boost both drag force and heat removal. Most importantly, temperature-dependent and space-dependent heat source/sink mechanisms exhibit a stronger influence on heat transport regulation, making them an important mode of thermal control. Overall, the results demonstrate that mixed convection flow is highly sensitive to nonlinear buoyancy and non-uniform heat generation/absorption. These findings provide useful insights for the design and optimization of thermal management systems across a wide range of engineering applications.

Keywords: Thermal energy transport, nonlinear buoyancy, moving vertical plate, partial slip, non-uniform heat source/sink.

1. Introduction

Boundary layer flow and the associated heat transfer over flat plates have attracted substantial attention due to their fundamental importance in widespread engineering applications, including electronic cooling, nuclear reactor thermal management, heat exchangers, coating processes, polymer extrusion, geothermal energy systems, and other manufacturing operations involving moving surfaces. The two classical boundary layer flow models are the Blasius flow model [1], which models a fixed flat plate in a moving fluid, and the Sakiadis flow model [2], which reports a moving plate in a still fluid. Their corresponding heat transfer characteristics were examined by

Pohlhausen [3] and Tsou *et al.* [4], respectively. To simultaneously represent the two aforementioned models involving both surface and ambient fluid velocities, Abdelhafez [5], Afzal et al. [6], Ishak [7] and Mukhopadhyay et al. [8] developed generalised formulations based on composite velocity boundary conditions. More recently, Dholey [9], Renuka et al. [10], and Khashi'ie et al. [11] further extended those models by scrutinizing the influence of various physical mechanisms on boundary layer flow and thermal transport over flat plates.

Convection is one of the primary modes of heat transfer in boundary layer flows, facilitating the exchange of thermal energy among a solid surface and the surrounding fluid. Based on the mechanism responsible for fluid motion, convection is generally categorised as forced, free (natural), or mixed convection. Forced convection occurs when the flow is generated by external devices such as pumps, fans, or moving surfaces, while free convection results from buoyancy forces produced by temperature-dependent density differences within the fluid. When both mechanisms act simultaneously, the resulting flow is referred to as mixed convection. In such cases, the combined influence of inertial and buoyancy forces may either assist or oppose the flow, depending on their relative directions. Mixed convection is encountered in numerous practical situations, including electronic cooling, heat exchangers, solar thermal systems, nuclear reactor cooling, geothermal applications, and atmospheric transport, making it an important topic of research [12]. Detailed studies on mixed convection boundary layer flows are available in Refs. [13–16].

Many previous investigations have been carried out within the framework of linear mixed convection by adopting the Boussinesq approximation, which assumes a linear variation of fluid density with temperature. This approximation is generally adequate when the temperature difference is small. However, its accuracy decreases as the temperature difference increases, since the density–temperature relationship becomes nonlinear. The resulting change in buoyancy force can substantially affect both the flow and heat transfer characteristics. As a result, predictions of velocity, temperature, wall drag force, and heat transfer rate based on the linear approximation may no longer be reliable. To capture these effects more accurately, nonlinear buoyancy models are required, particularly in high-temperature applications such as solar thermal systems, combustion chambers, nuclear reactors, thermal energy storage units, glass manufacturing, and high-temperature material processing.

To overcome the limitations of the linear Boussinesq approximation, Goren [17] introduced a quadratic density-temperature relation in the buoyancy term for free convection flows, making the model applicable to situations involving large temperature differences. Later, Bandaru et al. [18] extended this idea to mixed convection by incorporating both linear and quadratic density-temperature variations in the analysis of flow over a rotating cone in a porous medium. Their study showed that accounting for nonlinear buoyancy leads to a more realistic prediction of flow and heat transfer properties. Since then, nonlinear mixed convection has been investigated extensively because of its importance in thermal systems with large temperature gradients. Recent studies [19–22] have examined such flows over different configurations, including stretching surfaces, vertical plates, vertically moving cylinders, and wedges. These investigations have consistently shown that the nonlinear thermal buoyancy parameter has a much greater influence on the flow and temperature fields than the concentration-dependent buoyancy parameter, emphasizing its dominant role in boundary layer transport.

Internal heat generation and absorption have a pronounced effect on thermal transport in boundary layer flows by modifying the energy balance within the fluid. Heat generation increases the fluid temperature, resulting in a thicker thermal boundary layer and altering the wall temperature gradient, which directly affect the rate of heat transfer. In contrast, heat absorption removes thermal energy from the fluid, reducing the thermal boundary layer thickness and increasing the temperature gradient at the surface. Because buoyancy-driven flow in mixed convection is closely linked to the temperature field, the presence of a heat source or sink can significantly influence both the flow and heat transfer. These effects are important in many engineering applications, including electronic cooling, nuclear reactor thermal management, residual heat removal from nuclear debris, radioactive waste disposal, polymer extrusion, rubber and plastic processing, geothermal energy systems, chemical reactors, and various metallurgical and energy conversion processes. In such systems, proper regulation of internal heat generation or absorption is essential for maintaining thermal stability and improving overall performance.

Early investigations primarily focused on uniform heat source/sink models, in which the rate of internal heat generation or absorption depends only on the local temperature field. Such models were employed by Mukhopadhyay [23], Gireesha et al. [24], and Roy and Pop [25] to examine the influence of temperature-dependent heat generation/absorption on boundary layer heat transfer. Although these studies provided valuable insights into the role of internal heating and cooling, they assumed that the heat source/sink remained spatially uniform throughout the flow domain, which may not accurately represent many practical thermal systems. In realistic engineering processes, however, the intensity of internal heat generation or absorption often varies with both the local temperature and the spatial location due to non-uniform energy production, localized heating, chemical reactions, electromagnetic heating, radiation, or variable material properties. To capture these physical characteristics more accurately, several researchers, including Abel and Mahesha [26], Mythili and Sivaraj [27], Gireesha et al. [28], and Khan et al. [29], incorporated non-uniform heat source/sink models in which the internal heat generation/absorption is presumed to depend simultaneously on temperature and spatial coordinates. Such

models provide a more realistic representation of practical thermal systems and enable a better understanding of how localized energy generation or absorption influences the development of thermal boundary layers, wall heat transfer, and the overall transport process.

The no-slip boundary condition, which assumes that the fluid velocity at a solid surface is equal to the velocity of the surface, has been a basic assumption in continuum fluid mechanics for many years. It provides reliable predictions for most macroscopic flows, where the interaction between the fluid and the solid boundary is sufficiently strong to eliminate any relative motion at the interface. However, this assumption is not always valid in microscale and nanoscale systems. In applications involving rarefied gases, hydrophobic and superhydrophobic surfaces, porous or coated materials, polymeric fluids, and microelectromechanical systems (MEMS), finite slip may occur because of weak intermolecular interactions and limited momentum exchange near the wall. Gad-el-Hak [30] emphasized that neglecting slip effects in such situations can lead to significant errors in predicting flow and heat transfer characteristics. To account for these effects, the no-slip condition is replaced by a partial slip boundary condition that allows a finite tangential velocity at the wall. Navier [31] first proposed this model by relating the slip velocity to the tangential shear rate at the surface. A similar idea is used for heat transfer through the thermal slip, or temperature jump, condition, in which the temperature difference among the wall and the adjacent fluid is proportional to the normal temperature gradient. These boundary conditions provide a more realistic description of momentum and heat transfer at fluid–solid interfaces, particularly in microscale transport problems. In fact, velocity slip reduces the transfer of momentum from the wall to the fluid, leading to lower wall shear stress and changes in the momentum boundary layer. Likewise, thermal slip limits the amount of heat transferred from the surface to the nearby fluid, thereby decreasing the wall heat flux and modifying the thermal boundary layer. As a result, partial slip provides an effective way to regulate both flow resistance and heat transfer, which is particularly useful in microfluidic devices, MEMS/NEMS, biomedical applications, advanced cooling systems, lubrication, coating technologies, and energy conversion equipment. Owing to these practical advantages, slip boundary conditions have been widely adopted in studies of fluid flow and heat transfer [32–35]. For instance, Li et al. [36] examined magnetohydrodynamic flow with Navier slip under a modified heat conduction model and showed that wall slip reduces the surface cooling rate by lowering the wall heat flux. More recently, Uddin et al. [37] investigated unsteady mixed convection flow with velocity slip and activation energy, demonstrating that slip has a significant effect on both the flow and thermal fields. These studies underline the importance of incorporating velocity and thermal slip in the analysis of microscale flows and other situations where the classical no-slip assumption is no longer appropriate.

Motivated by the limitations of earlier studies, the present work investigates the combined effects of several physical mechanisms that have rarely been considered together in boundary layer flow and heat transfer. Unlike most previous investigations, which were limited to linear mixed convection, uniform heat generation/absorption, stationary surfaces, and no-slip boundary conditions, the present model considers nonlinear mixed convection over a vertically moving plate in the presence of a spatially-dependent and temperature-dependent heat source/sink, together with velocity and thermal slip at the wall. By accounting for nonlinear buoyancy, wall motion, non-uniform internal heat generation/absorption, and finite momentum and thermal exchange at the fluid–solid interface, the model provides a more realistic description of the transport processes. The interaction of these effects has a marked influence on the velocity and thermal boundary layers, wall shear stress, and surface heat transfer. The findings of this study are expected to be valuable in the design and analysis of advanced cooling systems, nuclear reactor thermal management, geothermal energy extraction, polymer processing, coating operations, microfluidic devices, and other thermal systems involving moving surfaces, internal heat generation, and slip effects. The results therefore provide useful insights into the design and optimization of thermal systems where precise control of fluid flow and heat transfer is essential.

The governing equations for the conservation of mass, momentum, and energy are first transformed into a system of coupled nonlinear ordinary differential equations using suitable similarity transformations. The transformed boundary value problem is then solved numerically with the MATLAB bvp4c solver, which has been widely used for nonlinear boundary layer problems because of its accuracy and reliability. A detailed parametric study is carried out to examine the effects of the governing parameters on the velocity and temperature distributions, skin-friction coefficient, and local Nusselt number. The results are presented through graphs and tables to clearly illustrate how the controlling parameters influence the flow and heat transfer characteristics.

The key novelty of this investigation comes from the combined and simultaneous consideration of several complex physical phenomena which have not been addressed together previously:

(a) Incorporation of nonlinear mixed convection with temperature-dependent and space-dependent non-uniform heat source/sink, permitting a more realistic representation of internal heating designs found in advanced thermal systems.

(b) Inclusion of both velocity slip and thermal jump boundary conditions, accounting for microscale surface interactions that considerably alter transport phenomena near the plate.

(c) Coupling of a moving vertical plate with buoyancy-driven effects, producing a multi-driving force flow environment that introduces additional nonlinear behaviour.

(d) Detailed quantification of competing thermal and momentum transport mechanisms, revealing how slip, heat source/sink strength, buoyancy, and wall motion interact to shape shear stress and heat transfer characteristics.

To the best of the authors' knowledge, such a combination of nonlinear mixed convection, non-uniform heat source/sink, moving surface, and dual slip boundary conditions has not been previously reported, and thus provides new physical insights into boundary-layer transport phenomena relevant to modern thermal engineering applications.

2. Formulation and basic equations

Consider the steady-state non-linear buoyancy-driven mixed convection over a vertical plate incorporating non-uniform heat source/sink. The *x*-axis is taken along the plate, while the *y*-axis is considered perpendicular to it. Governing equations within boundary layer are specified as [21, 22, 24]:

$$\frac{\partial u}{\partial x}+\frac{\partial v}{\partial y}=0\,, \tag{1}$$

$$u\frac{\partial u}{\partial x}+v\frac{\partial v}{\partial y}=\upsilon\frac{\partial^2 u}{\partial y^2}+g[\beta_0(T-T_\infty)+\beta_1(T-T_\infty)^2]\,, \tag{2}$$

$$u\frac{\partial T}{\partial x}+v\frac{\partial T}{\partial y}=\frac{\kappa}{(\rho c_p)}\frac{\partial^2 T}{\partial y^2}+\frac{1}{\rho c_p}q^*\,, \tag{3}$$

with boundary conditions(BCs)

$$u=U_w+L_1\frac{\partial u}{\partial y}, v=0 \text{ at } y=0\,,\ u\to 0 \text{ as } y\to\infty\,, \tag{4}$$

$$T=T_w+D_1\frac{\partial T}{\partial y} \text{ at } y=0\,,\ T\to T_\infty \text{ as } y\to\infty, \tag{5}$$

where u and v are the velocity components along *x*- and *y*-axes, respectively, T gives the temperature, $\upsilon=\mu/\rho$ denotes the kinematic viscosity, β_0 and β_1 represent linear and nonlinear thermal expansion coefficients, T_w and T_∞ respectively give the constant temperatures at the plate and in the free-stream with $T_w>T_\infty$, U_w is surface velocity, g is the acceleration due to gravity, and κ, (ρc_p), μ, and ρ are the thermal conductivity, heat capacity, viscosity, and density, respectively. Here, $L_1=L\,\mathrm{Re}_x^{1/2}$ and $D_1=D\,\mathrm{Re}_x^{1/2}$ are the velocity slip and thermal slip factors with L and D being the initial values of L_1 and D_1 having dimension of length, and $\mathrm{Re}_x=U_w x/\upsilon$ gives the local Reynolds number. The physical layout of the problem being investigated is depicted in Figure 1.

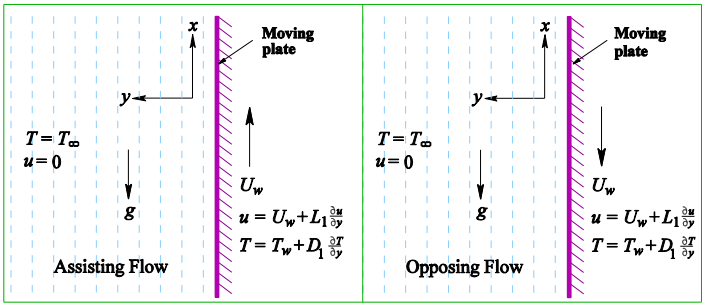


Figure 1. Physical diagram of considered problem.

The adopted heat generation/absorption model represents a non-uniform internal heat source/sink whose strength depends on both the local fluid temperature and the spatial location within the boundary layer. It is more realistic than the conventional uniform heat source/sink model because, in many practical thermal systems, heat is neither generated nor absorbed uniformly throughout the flow domain.

The dimensional heat source/sink is expressed as [24, 27]:

$$q^* = \frac{\kappa U_w}{\upsilon x}\left[q_1(T - T_\infty) + q_2(T_w - T_\infty) e^{-\frac{y}{x}\sqrt{\frac{U_w x}{\upsilon}}} \right]. \tag{6}$$

The term $q_1(T - T_\infty)$ implies that the rate of internal heat generation (or absorption) varies with the local temperature difference among the fluid and the ambient environment. Whereas, the $q_2(T_w - T_\infty)e^{-\frac{y}{x}\sqrt{\frac{U_w x}{\upsilon}}}$ term refers to the spatial variation of the heat source/sink and the exponential function decreases rapidly as the distance from the wall increases. Therefore, maximum heat generation (or absorption) occurs near the wall and the source/sink gradually weakens away from the surface. Here, q_1 and q_2 are coefficients of temperature-dependent and space-dependent heat source/sink, respectively. It should be noted that $q_1 > 0$, $q_2 > 0$ produces heat source and $q_1 < 0$, $q_2 < 0$ represents heat sink. These two parameters control the strength of the two mechanisms independently.

The following transformations are employed:

$$\psi = \sqrt{U_w \upsilon x} f(\eta) \text{ and } T = T_\infty + (T_w - T_\infty)\theta(\eta), \tag{7}$$

where $\eta = (y/x)\mathrm{Re}_x^{1/2}$ is a variable, f and θ are dimensionless functions.

Using aforementioned transformations, the equations and BCs reduce to

$$f''' + \frac{1}{2} f f'' + \lambda\theta(1 + \gamma\theta) = 0, \tag{8}$$

$$\theta'' + \frac{1}{2}\mathrm{Pr}\, f\theta' + q_1\theta + q_2 e^{-\eta} = 0, \tag{9}$$

with

$$f(0) = 0,\ f'(0) = 1 + \delta_1 f''(0),\ f'(\infty) = 0, \tag{10}$$

$$\theta(0) = 1 + \delta_2\theta'(0),\ \theta(\infty) = 0, \tag{11}$$

where $\lambda = \frac{Gr_x}{\mathrm{Re}_x^2}$, $Gr_x = \frac{g\beta_0(T_w - T_\infty)x^3}{\upsilon^2}$, $\gamma = \frac{\beta_1}{\beta_0}(T_w - T_\infty)$, $\mathrm{Pr} = \frac{\upsilon\rho c_p}{\kappa}$, $\delta_1 = \frac{LU_w}{\upsilon}$ and $\delta_2 = \frac{DU_w}{\upsilon}$ are the linear buoyancy parameter, local Grashof number, nonlinear convection parameter, Prandtl number, velocity and thermal slip parameters, respectively.

The local skin-friction coefficient and Nusselt number, representing the shear stress and heat transfer rate at the surface, respectively, are defined in standard form as follows:

$$C_{fx} = \frac{\tau_w}{\rho U_w^2} \text{ and } Nu_x = \frac{x q_w}{\kappa\left(T_w - T_\infty\right)}, \tag{12}$$

where $\tau_w = \mu\left(\frac{\partial u}{\partial y}\right)_{y=0}$ and $q_w = -\kappa\left(\frac{\partial T}{\partial y}\right)_{y=0}$.

So, above quantities reduce to

$$\left.\begin{aligned} \mathrm{Re}^{1/2} C_{fx} &= f''(0), \\ \mathrm{Re}^{-1/2} Nu_x &= -\theta'(0). \end{aligned}\right\} \tag{13}$$

3. Solution methodology and its validations

The coupled nonlinear ODEs given in Eqs. (8)-(11) are solved using 'bvp4c', a MATLAB program which is built on Lobatto IIIA technique (a finite difference scheme producing C^1-continuous solutions). This approach minimizes sensitivity to starting estimates by automatically adapting the computational mesh for accuracy and offering reliable results even in the absence of closed-form initial assumptions. Boundary value problems in bvp4c are solved using the setting sol=bvp4c(odefun, bcfun,solinit,options). In this case, odefun stores the system of first-order ordinary differential equations, bcfun specifies the boundary conditions, solinit describes the initial guess values, and options=bvpset('RelTol',1e-6, 'AbsTol',1e-6) is used to establish the relative and absolute error tolerances.

Since the bvp4c is applied on a first order system, the Eqs. (8)-(11) are transformed into the following first-order system:

$$\left.\begin{aligned} f' = g,\ g' = h,\ h' = -\frac{1}{2} fh - \lambda\theta\left(1+\gamma\theta\right), \\ \theta' = \Theta,\ \Theta' = -\frac{1}{2}\Pr f\Theta - q_1\theta - q_2 e^{-\eta}, \end{aligned}\right\} \tag{14}$$

with

$$f(0) = 0,\ g(0) = 1+\delta_1 h(0),\ \theta(0) = 1+\delta_2\Theta(0). \tag{15}$$

To start integration, introductory guess values of non-prescribed initial conditions $h(0)$ and $\Theta(0)$, i.e., $f''(0)$ and $\theta'(0)$ are essential and the values are selected in such a manner that they produce asymptotic convergence to specified boundary conditions. Here, the error is determined by the residual error with tolerance being 10^{-5}.

To validate the accuracy of the present numerical methodology, the computed values of the skin-friction coefficient $\mathrm{Re}^{1/2} C_{fx}$ for the forced convection case are compared with the previously reported results of Bataller [38], Ahmad et al. [39], and Rahman et al. [40], as presented in Table 1. An excellent agreement is observed between the present computations and the available benchmark solutions over the entire range of parameters considered. This close correspondence approves the accuracy and dependability of the adapted numerical procedure, thereby providing strong confidence in the correctness of the results and the subsequent physical interpretations presented in this study.

Table 1. Comparison of skin-friction coefficient $\mathrm{Re}^{1/2} C_{fx}$ for $\lambda = 0$.

δ_1	Bataller [38]	Ahmad et al. [39]	Rahman et al. [40]	Present results
0	0.4437	0.4446	0.4438	0.4439043
0.2			0.3925	0.3927017
0.4			0.3531	0.3533116

4. Results and discussion

The governing mathematical model is solved numerically to examine the underlying flow physics. Furthermore, a detailed parametric examination is conducted to assess the effects of the linear and nonlinear mixed convection parameters, temperature-dependent and space-dependent heat source/sink, and velocity and thermal slips on the velocity and temperature fields, together with the corresponding wall drag force and rate of surface cooling, as exhibited in Figures 2-25. Throughout the numerical computations, the parameter values are fixed as: $\lambda = 0.1$, $\gamma = 0.5$, $q_1 = 0.04$, $q_2 = 0.1$, $\delta_1 = 0.2$, $\delta_2 = 0.1$ and ($q_1 = -0.04$, $q_2 = -0.1$, in case of a sink). Unless otherwise specified, these values remain unchanged.

The effects of varying the convection parameters on the velocity and temperature profiles are illustrated in Figures 2-5. Here, $\lambda < 0$, $\lambda > 0$, and $\lambda = 0$ correspond to opposing, assisting, and forced convection flows, respectively. The fluid velocity rises with an increase in the linear mixed convection parameter under assisting flow conditions $(\lambda > 0)$ as demonstrated by Figure 2. This enhancement occurs because the buoyancy force acts in the identical direction as the main flow, accelerating the fluid, raising the momentum boundary layer thickness (BLT), and producing a more favourable flow environment. In contrast, under opposing flow situations $(\lambda < 0)$, the buoyancy force executes against the fluid motion, thereby decelerating the flow and thinning the momentum boundary layer. Consequently, the velocity attained in the forced convection case $(\lambda = 0)$ lies between those of the assisting and opposing flow regimes. The corresponding temperature distributions are presented in Figure 3. An opposite trend is observed with respect to the velocity field. As the linear mixed convection parameter grows, the temperature and thermal BLT decrease because the accelerated fluid transports heat away from the surface more effectively, thereby enhancing convective heat transfer. Conversely, the decelerated flow in the opposing convection regime weakens convective transport, allowing more thermal energy to collect within the boundary layer, which produces higher temperature of fluid and a thicker thermal boundary layer. Accordingly, the temperature in the forced convection case remains lower than that in opposing flow but higher than that in assisting flow.

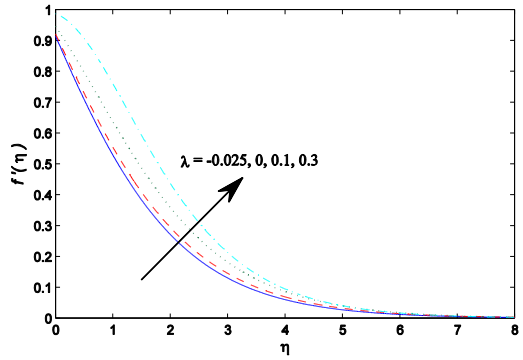


Figure 2. Variations in $f'(\eta)$ for several λ with $\gamma = 0.5$, $q_1 = 0.04$, $q_2 = 0.1$, $\delta_1 = 0.2$, $\delta_2 = 0.1$.

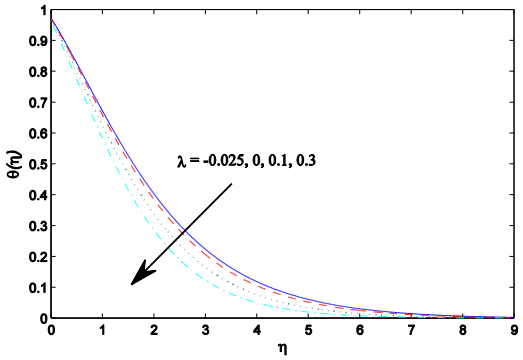


Figure 3. Variations in $\theta(\eta)$ for several λ with $\gamma = 0.5$, $q_1 = 0.04$, $q_2 = 0.1$, $\delta_1 = 0.2$, $\delta_2 = 0.1$.

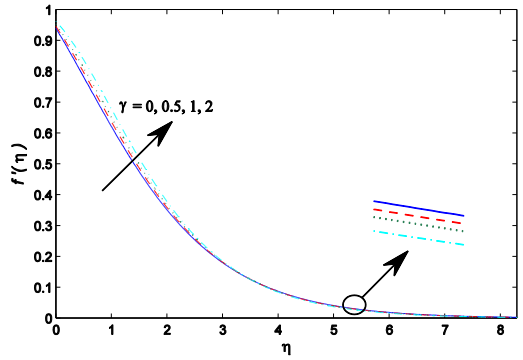


Figure 4. Variations in $f'(\eta)$ for several γ with $\lambda = 0.1$, $q_1 = 0.04$, $q_2 = 0.1$, $\delta_1 = 0.2$, $\delta_2 = 0.1$.

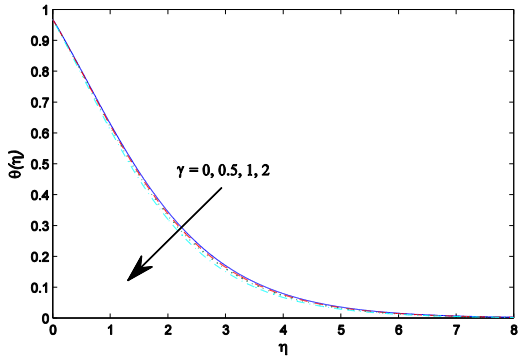


Figure 5. Variations in $\theta(\eta)$ for several γ with $\lambda = 0.1$, $q_1 = 0.04$, $q_2 = 0.1$, $\delta_1 = 0.2$, $\delta_2 = 0.1$.

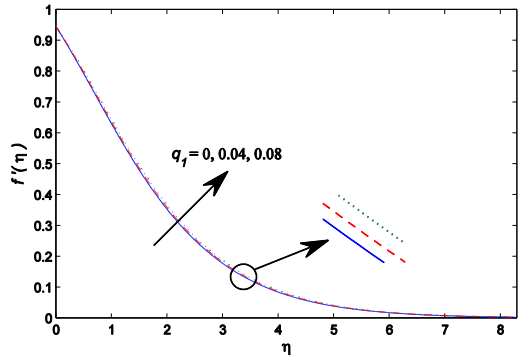


Figure 6. Variations in $f'(\eta)$ for several $q_1(\geq 0)$ with $\lambda = 0.1$, $\gamma = 0.5$, $q_2 = 0.1$, $\delta_1 = 0.2$, $\delta_2 = 0.1$.

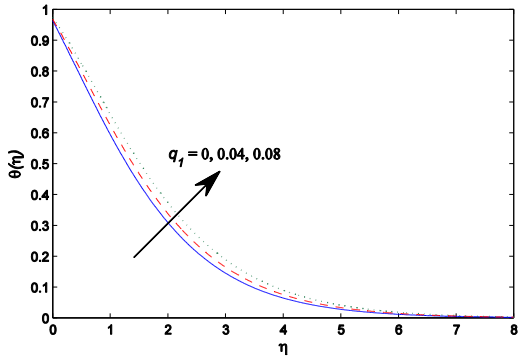


Figure 7. Variations in $\theta(\eta)$ for several $q_1(\geq 0)$ with $\lambda = 0.1$, $\gamma = 0.5$, $q_2 = 0.1$, $\delta_1 = 0.2$, $\delta_2 = 0.1$.

The effects of the nonlinear mixed convection parameter (γ) on the velocity and temperature distributions are illustrated in Figures 4 and 5. It is worth mentioning that ($\gamma = 0$) corresponds to the classical linear mixed convection model. As γ increases, the velocity exhibits a non-uniform response: the fluid velocity increases in the vicinity of the surface, whereas it declines in the outer region of the boundary layer. This performance is attributed to the nonlinear dependence of the buoyancy force on temperature. Near the heated plate, where the temperature difference among the wall and the nearby fluid is huge, the resulting nonlinear buoyancy force becomes stronger, producing an additional driving force that accelerates the fluid motion. However, as the distance from the surface increases, the temperature difference reduces quickly, consequently causing the nonlinear buoyancy effect to weaken. Hence, the momentum produced by buoyancy becomes inadequate to sustain the enhanced flow, leading to a decrease in velocity in the far-field region. Figure 5 unveils that raising the nonlinear mixed convection parameter diminishes both the fluid temperature and the thermal BLT. The strengthened near-wall buoyancy rushes the fluid motion, which promotes stronger convective transport of thermal energy away from the heated plate wall and accordingly it suppresses the thermal boundary layer development. Furthermore, the temperature and thermal

boundary layer are in higher level for the linear convection case $(\gamma = 0)$ than for the nonlinear convection case. In the linear model, the buoyancy force changes in direct proportion to temperature, whereas the nonlinear model produces a stronger buoyancy force in the high-temperature region near the wall. As the fluid temperature gradually approaches the free-stream value, the nonlinear buoyancy effect weakens. Consequently, nonlinear convection transfers heat more efficiently in the near-wall region, resulting in lower fluid temperatures and a thinner thermal boundary layer.

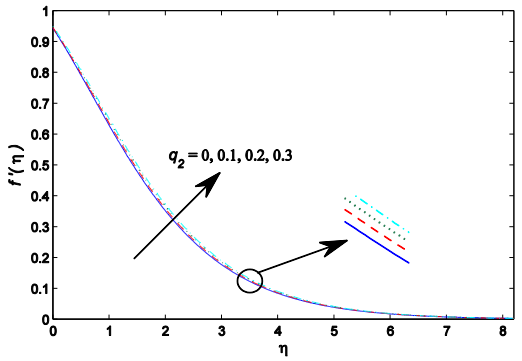


Figure 8. Variations in $f'(\eta)$ for several $q_2(\geq 0)$ with $\lambda = 0.1,\ \gamma = 0.5,\ q_1 = 0.04,\ \delta_1 = 0.2,\ \delta_2 = 0.1$.

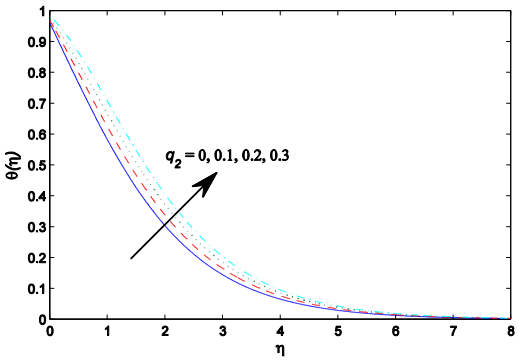


Figure 9. Variations in $\theta(\eta)$ for several $q_2(\geq 0)$ with $\lambda = 0.1,\ \gamma = 0.5,\ q_1 = 0.04,\ \delta_1 = 0.2,\ \delta_2 = 0.1$.

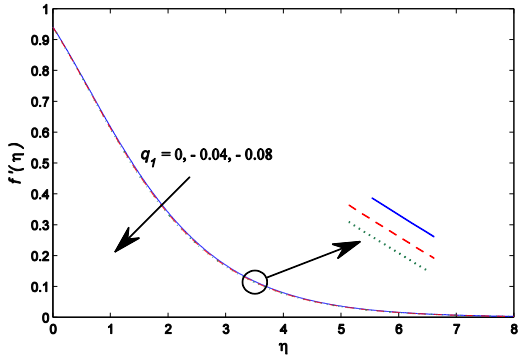


Figure 10. Variations in $f'(\eta)$ for several $q_1(\leq 0)$ with $\lambda = 0.1,\ \gamma = 0.5,\ q_2 = -0.1,\ \delta_1 = 0.2,\ \delta_2 = 0.1$.

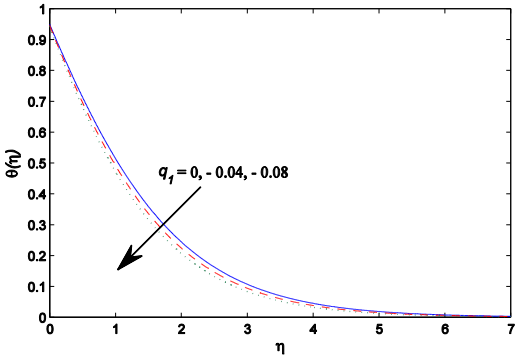


Figure 11. Variations in $\theta(\eta)$ for several $q_1(\leq 0)$ with $\lambda = 0.1,\ \gamma = 0.5,\ q_2 = -0.1,\ \delta_1 = 0.2,\ \delta_2 = 0.1$.

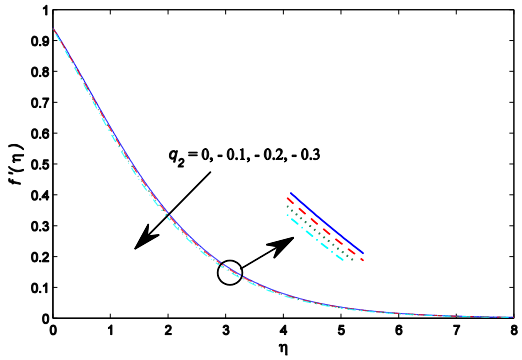


Figure 12. Variations in $f'(\eta)$ for several $q_2(\leq 0)$ with $\lambda = 0.1,\ \gamma = 0.5,\ q_1 = -0.04,\ \delta_1 = 0.2,\ \delta_2 = 0.1$.

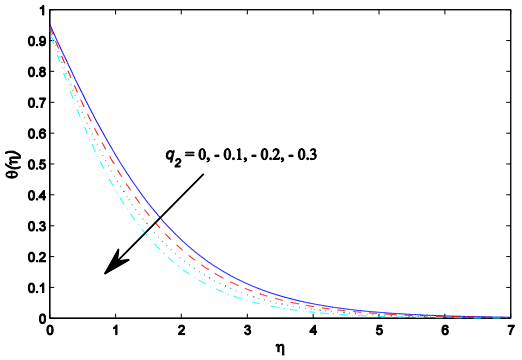


Figure 13. Variations in $\theta(\eta)$ for several $q_2(\leq 0)$ with $\lambda = 0.1,\ \gamma = 0.5,\ q_1 = -0.04,\ \delta_1 = 0.2,\ \delta_2 = 0.1$.

The variations of velocity and temperature distributions with the temperature-dependent and space-dependent heat source/sink parameters are depicted in Figures 6-13. In the presence of a heat source, both the velocity and temperature upsurge, whereas the opposite trend is observed when there is a heat sink. This impact is a direct consequence of the modification of the thermal energy within the boundary layer. Moreover, the presence of a heat source uninterruptedly supplies thermal energy to the fluid, causing temperature hike by strengthening the thermal buoyancy force. The enhanced buoyancy produces acceleration in the fluid flow, which causes higher velocities and a thicker momentum boundary layer. On the contrary, a heat sink removes thermal energy from the fluid,

which reduces the temperature difference among the wall and the nearby fluid and the weaker buoyancy force causes a reduction in the fluid velocity throughout the boundary layer. The corresponding temperature distributions exhibit that both the temperature-dependent and space-dependent heat source/sink parameters produce similar influences on the thermal variations. Increasing any source parameter introduces extra heat into the fluid, causing the rise of temperature and a larger thermal BLT. In contrast, increasing the strength of either heat sink parameter enhances heat absorption from the fluid, thereby suppressing the thermal distribution, reducing the thermal BLT, and promoting a steeper temperature gradient at the wall. From a heat transfer perspective, the heat source weakens the wall heat transfer rate by increasing the thermal energy within the boundary layer, whereas the heat sink intensifies this wall heat transfer through the continuous removal of thermal energy from the fluid. Consequently, the thermal boundary layer becomes thicker in the presence of a heat source and thinner when a heat sink is applied.

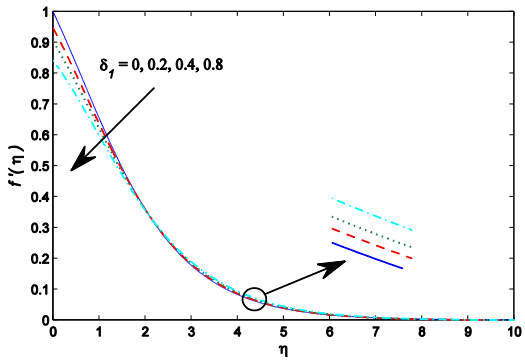


Figure 14. Variations in $f'(\eta)$ for several δ_1 with $\lambda = 0.1$, $\gamma = 0.5$, $q_1 = 0.04$, $q_2 = 0.1$, $\delta_2 = 0.1$.

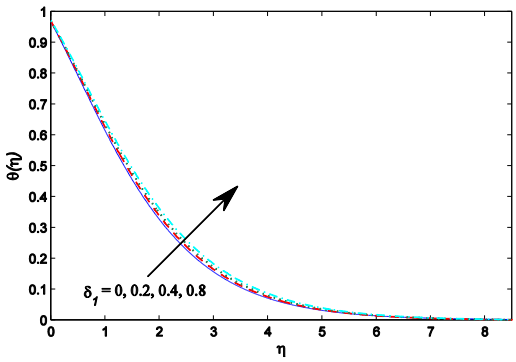


Figure 15. Temperature $\theta(\eta)$ for various δ_1 with $\lambda = 0.1$, $\gamma = 0.5$, $q_1 = 0.04$, $q_2 = 0.1$, $\delta_2 = 0.1$.

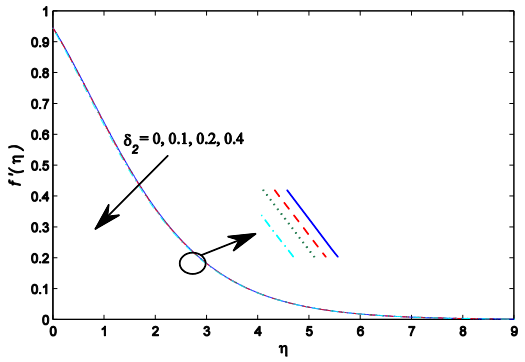


Figure 16. Variations in $f'(\eta)$ for several δ_2 with $\lambda = 0.1$, $\gamma = 0.5$, $q_1 = 0.04$, $q_2 = 0.1$, $\delta_1 = 0.2$.

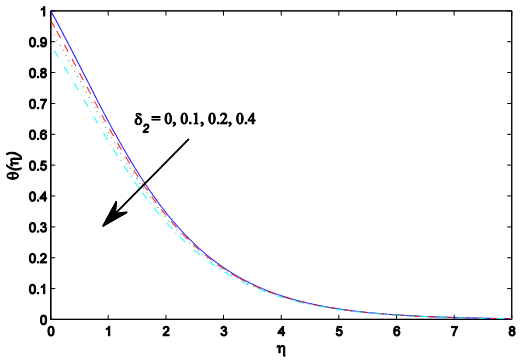


Figure 17. Temperature $\theta(\eta)$ for various δ_2 with $\lambda = 0.1$, $\gamma = 0.5$, $q_1 = 0.04$, $q_2 = 0.1$, $\delta_1 = 0.2$.

The differences in velocity and temperature due to changes in the velocity and thermal slip parameters are demonstrated in Figures 14-17. It should be noted that the present slip model reduces to the classical no-slip/no-temperature-jump boundary condition when the corresponding slip parameters are set to zero. The results in Figure 14 establish that increasing the velocity slip parameter produces a dual effect on the velocity field. In the vicinity of the wall, the fluid velocity decreases because the tangential slip weakens the momentum transfer from the moving surface to the adjacent fluid layers. As a result, the wall exerts less shear stress on the fluid, reducing its acceleration near the boundary. However, farther away from the surface, the velocity becomes slightly higher than that of the no-slip case owing to the redistribution of momentum within the boundary layer. The reduced wall friction delays the decay of the fluid motion, thereby yielding relatively higher velocities in the outer region of the boundary layer. Increasing the velocity slip parameter uplifts the fluid temperature and increases the thermal BLT (Figure 15). This behaviour arises because the weakened momentum transfer suppresses fluid mixing and convective heat transport near the wall, allowing heat energy to gather inside the boundary layer. Consequently, the thermal diffusion process becomes more dominant, resulting in higher temperatures throughout the flow field.

The impact of thermal slip (thermal jump) is presented in Figures 16 and 17. It is observed that increasing the thermal slip parameter reduces both the fluid velocity and temperature. Physically, thermal slip introduces a finite temperature discontinuity at the wall, thereby reducing the amount of heat transferred from the surface to the adjacent fluid. The reduction in thermal energy weakens the buoyancy force, which drives the mixed convection flow and due to this weaker buoyancy force fluid velocity reduces. At the same time, the decrease in wall heat flux suppresses the thermal field, generating a noticeable reduction in the fluid temperature and in the thermal BLT.

This cooling effect is more dominant near the wall, where the thermal slip condition restricts heat transfer from the surface to the adjacent fluid. As the distance from the wall increases, the influence of thermal slip gradually diminishes because the fluid temperature progressively approaches the ambient value.

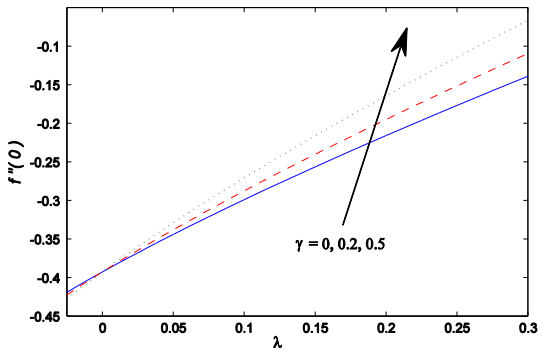


Figure 18. Local skin-friction $f''(0)$ with λ for various γ with $q_1 = 0.04,\ q_2 = 0.1,\ \delta_1 = 0.2,\ \delta_2 = 0.1$.

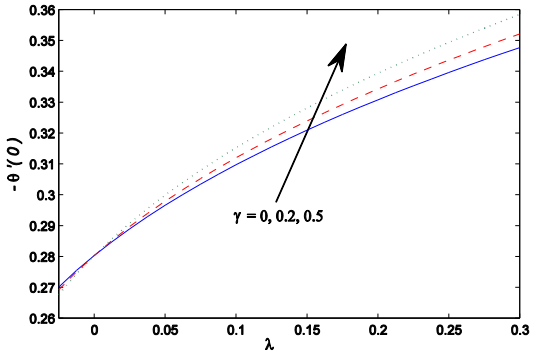


Figure 19. Local Nusselt number $-\theta'(0)$ with λ for various γ with $q_1 = 0.04,\ q_2 = 0.1,\ \delta_1 = 0.2,\ \delta_2 = 0.1$.

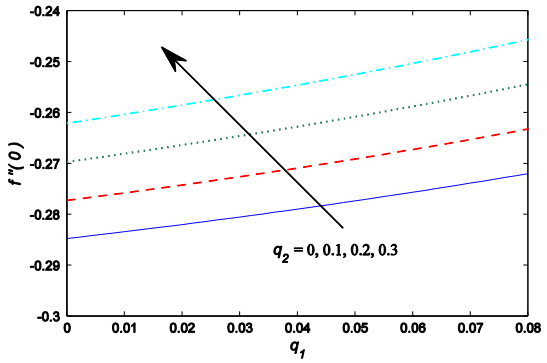


Figure 20. Local skin-friction $f''(0)$ with $q_1(\geq 0)$ for various $q_2(\geq 0)$ with $\lambda = 0.1,\ \gamma = 0.5,\ \delta_1 = 0.2,\ \delta_2 = 0.1$.

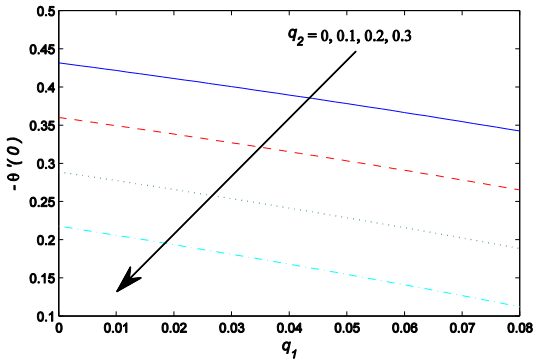


Figure 21. Local Nusselt number $-\theta'(0)$ with $q_1(\geq 0)$ for various $q_2(\geq 0)$ with $\lambda = 0.1,\ \gamma = 0.5,\ \delta_1 = 0.2,\ \delta_2 = 0.1$.

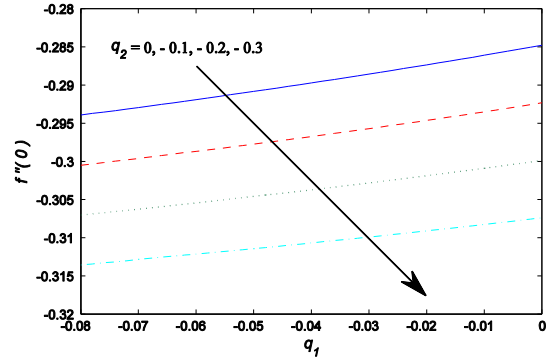


Figure 22. Local skin-friction $f''(0)$ with $q_1(\leq 0)$ for various $q_2(\leq 0)$ with $\lambda = 0.1,\ \gamma = 0.5,\ \delta_1 = 0.2,\ \delta_2 = 0.1$.

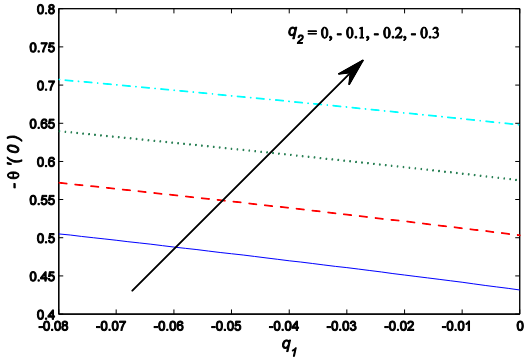


Figure 23. Local Nusselt number $-\theta'(0)$ with $q_1(\leq 0)$ for various $q_2(\leq 0)$ with $\lambda = 0.1,\ \gamma = 0.5,\ \delta_1 = 0.2,\ \delta_2 = 0.1$.

Finally, the impacts of the linear and nonlinear mixed convection parameters, temperature-dependent and space-dependent heat source/sink parameters, and partial velocity and thermal slips on the engineering quantities of practical interest, namely the surface drag force and the heat transfer rate at the wall are exemplified Figures in 18-25. It is witnessed that under assisting flow conditions, increasing either the linear or nonlinear mixed convection parameter diminishes the magnitude of the surface drag force while simultaneously enhancing the rate of heat transport from the heated wall. In assisting flow, the buoyancy force acts in the direction of the externally driven flow, thereby accelerating the fluid and reducing the velocity gradient at the wall, which lowers the wall shear stress. At the same time, the stronger fluid motion intensifies convective heat transport, resulting in a sharper temperature gradient at the wall and hence a higher Nusselt number. In the opposing flow case, the buoyancy force acts against the primary flow which originates a decline in the fluid motion and an increment in the wall shear

stress. The reduced convective transport also produces a lower wall heat transfer rate. These effects become more pronounced near the heated wall, where the larger temperature difference gives rise to stronger nonlinear buoyancy. Consequently, nonlinear mixed convection has a significant influence on both the wall drag force and the heat transfer rate at the wall.

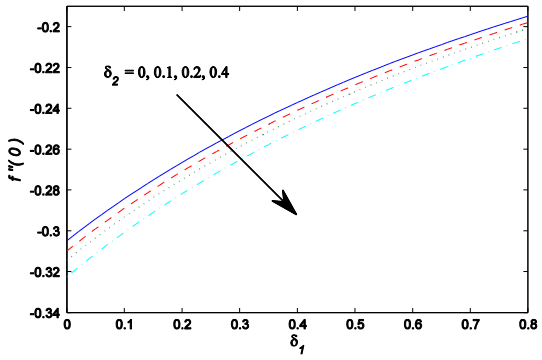


Figure 24. Local skin-friction $f''(0)$ with δ_1 for various δ_2 with $\lambda = 0.1,\ \gamma = 0.5,\ q_1 = 0.04,\ q_2 = 0.1$.

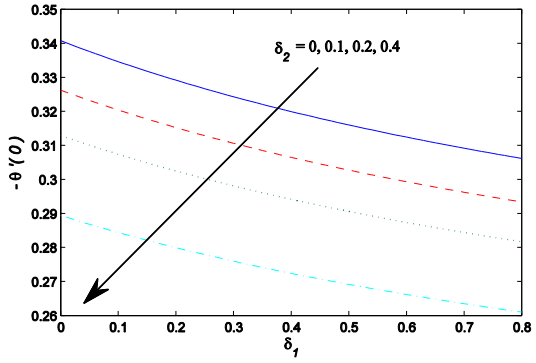


Figure 25. Local Nusselt number $-\theta'(0)$ with δ_1 for various δ_2 with $\lambda = 0.1,\ \gamma = 0.5,\ q_1 = 0.04,\ q_2 = 0.1$.

The influences of the temperature-dependent and space-dependent heat source/sink parameters on the engineering quantities are portrayed in Figures 20-23. It is evident that growing the strengths of both heat sources causes a decrease in the magnitude of the skin-friction coefficient, whereas the opposite trend is witnessed for the heat sink. Physically, the additional thermal energy added by the heat source uplifts the fluid temperature and increases the thermal BLT. This accumulation of heat energy weakens the wall velocity gradient, which reduces the surface drag exerted by the surface on the fluid. Conversely, a heat sink nonstop removes heat energy from the fluid, which reduces the thermal BLT and produces an increment in velocity gradient near the wall, i.e., the skin-friction coefficient. Similarly, the presence of a heat source reduces the wall temperature gradient because the heat energy is gathered within the boundary layer, which results in a lower Nusselt number. In contrast, a heat sink endlessly removes heat energy from the fluid, which promotes more efficient surface cooling, i.e., increases the rate of heat transfer.

The influences of velocity and thermal slips on the wall shear stress and heat transfer rate are exhibited in Figures 24 and 25. With a larger the velocity slip parameter, the magnitude of the skin-friction coefficient decreases because the slip boundary condition decays the transfer of tangential momentum from the wall to the fluid and it reduces the wall shear stress. In contrast, with increasing values of the thermal slip parameter, the skin-friction coefficient intensifies. Since thermal slip limits the transfer of heat from the wall to the nearby fluid, the buoyancy force reduces. Accordingly, this slows down the fluid motion and produces a superior wall drag force. In addition, increments of both velocity and thermal slip parameters reduce the local Nusselt number. Velocity slip reduces convective transport by dipping the momentum transport from the wall to the fluid, while thermal slip introduces a finite temperature jump at the wall, which diminishes the wall heat transfer rate.

The numerical values of the skin-friction coefficient and the local Nusselt number for different combinations of the governing parameters are presented in Table 2. These results are in close agreement with the graphical observations and this reconfirms of the trends discussed earlier regarding the impacts of the physical parameters on the flow field and thermal transport.

5. Conclusions and future research

The present study examines thermal energy transport in nonlinear mixed convection flow of a viscous fluid over a vertically moving plate in the presence of a temperature-dependent and space-dependent heat source/sink. To provide a more realistic description of the fluid-solid interface, the classical no-slip boundary conditions are replaced with partial velocity and thermal slip conditions. The resulting nonlinear boundary value problem is solved numerically using the MATLAB “bvp4c” solver, and the influences of the governing parameters on the flow and thermal fields, skin-friction coefficient, and heat transfer rate are analyzed in detail through graphical and numerical results. The major findings of the current investigation are summarized as follows:

- The linear mixed convection parameter has a significant influence on the flow and heat transfer characteristics. In the assisting flow case, the buoyancy force enhances the fluid motion, reduces the thickness of the momentum boundary layer, and improves the wall cooling rate. In contrast, opposing flow weakens the fluid motion, thickens the momentum boundary layer, and reduces the surface heat transfer rate.

Table 2. The values of $\mathrm{Re}^{1/2} C_{fx}$ and $\mathrm{Re}^{-1/2} Nu_x$ for the parameters λ, γ, q_1, q_2, δ_1, δ_2 and Pr.

λ	γ	q_1	q_2	δ_1	δ_2	Pr	$f''(0)$	$-\theta'(0)$
-0.025	0.5	0.04	0.1	0.2	0.1	1	-0.42771733	0.26760789
-0.01	0.5	0.04	0.1	0.2	0.1	1	-0.40637026	0.27552261
0	0.5	0.04	0.1	0.2	0.1	1	-0.39270177	0.28026413
0.1	0.5	0.04	0.1	0.2	0.1	1	-0.27085974	0.31522155
0.2	0.5	0.04	0.1	0.2	0.1	1	-0.16425981	0.33935216
0.3	0.5	0.04	0.1	0.2	0.1	1	-0.06633702	0.35845010
0.1	0	0.04	0.1	0.2	0.1	1	-0.29905004	0.30969727
0.1	0.25	0.04	0.1	0.2	0.1	1	-0.28486048	0.31250381
0.1	0.5	0.04	0.1	0.2	0.1	1	-0.27085974	0.31522155
0.1	0.75	0.04	0.1	0.2	0.1	1	-0.25703658	0.31785711
0.1	1	0.04	0.1	0.2	0.1	1	-0.24338094	0.32041637
0.1	1.25	0.04	0.1	0.2	0.1	1	-0.22988373	0.32290455
0.1	1.5	0.04	0.1	0.2	0.1	1	-0.21653675	0.32532632
0.1	1.75	0.04	0.1	0.2	0.1	1	-0.20333252	0.32768587
0.1	2	0.04	0.1	0.2	0.1	1	-0.19026425	0.32998699
0.1	0.5	-0.02	-0.1	0.2	0.1	1	-0.29463241	0.52187413
0.1	0.5	-0.04	-0.1	0.2	0.1	1	-0.29674266	0.53942356
0.1	0.5	-0.06	-0.1	0.2	0.1	1	-0.29870189	0.55626739
0.1	0.5	-0.08	-0.1	0.2	0.1	1	-0.30051242	0.57247451
0.1	0.5	0	0.1	0.2	0.1	1	-0.27722275	0.36006792
0.1	0.5	0.02	0.1	0.2	0.1	1	-0.27418990	0.33823133
0.1	0.5	0.04	0.1	0.2	0.1	1	-0.27085974	0.31522155
0.1	0.5	0.06	0.1	0.2	0.1	1	-0.26721264	0.29088397
0.1	0.5	0.08	0.1	0.2	0.1	1	-0.25943242	0.26287313
0.1	0.5	-0.04	-0.05	0.2	0.1	1	-0.29323511	0.50466836
0.1	0.5	-0.04	-0.1	0.2	0.1	1	-0.29674266	0.53942356
0.1	0.5	-0.04	-0.15	0.2	0.1	1	-0.30024249	0.57423564
0.1	0.5	-0.04	-0.2	0.2	0.1	1	-0.30373453	0.60910534
0.1	0.5	-0.04	-0.25	0.2	0.1	1	-0.30721875	0.64403345
0.1	0.5	-0.04	-0.3	0.2	0.1	1	-0.31068077	0.67901834
0.1	0.5	0.04	0	0.2	0.1	1	-0.27900698	0.38945331
0.1	0.5	0.04	0.05	0.2	0.1	1	-0.27493326	0.35228947
0.1	0.5	0.04	0.1	0.2	0.1	1	-0.27085974	0.31522155
0.1	0.5	0.04	0.15	0.2	0.1	1	-0.26678615	0.27824730
0.1	0.5	0.04	0.2	0.2	0.1	1	-0.26271225	0.24136462
0.1	0.5	0.04	0.25	0.2	0.1	1	-0.25863780	0.20457151
0.1	0.5	0.04	0.3	0.2	0.1	1	-0.25456261	0.16786604
0.1	0.5	0.04	0.1	0	0.1	1	-0.30987824	0.32623277
0.1	0.5	0.04	0.1	0.1	0.1	1	-0.28896798	0.32038814
0.1	0.5	0.04	0.1	0.2	0.1	1	-0.27085974	0.31522155
0.1	0.5	0.04	0.1	0.3	0.1	1	-0.25500365	0.31061414
0.1	0.5	0.04	0.1	0.4	0.1	1	-0.24098880	0.30647463
0.1	0.5	0.04	0.1	0.5	0.1	1	-0.22850113	0.30273144
0.1	0.5	0.04	0.1	0.6	0.1	1	-0.21729591	0.29932748
0.1	0.5	0.04	0.1	0.7	0.1	1	-0.20717930	0.29621655
0.1	0.5	0.04	0.1	0.8	0.1	1	-0.19799550	0.29336080
0.1	0.5	0.04	0.1	0.2	0	1	-0.26649202	0.32915924
0.1	0.5	0.04	0.1	0.2	0.1	1	-0.27085974	0.31522155
0.1	0.5	0.04	0.1	0.2	0.2	1	-0.27484186	0.30246671
0.1	0.5	0.04	0.1	0.2	0.3	1	-0.27848853	0.29074521
0.1	0.5	0.04	0.1	0.2	0.4	1	-0.28184136	0.27993238
0.1	0.5	0.04	0.1	0.2	0.1	0.5	-0.21568045	0.14050573
0.1	0.5	0.04	0.1	0.2	0.1	1	-0.27085974	0.31522155
0.1	0.5	0.04	0.1	0.2	0.1	1.5	-0.29540403	0.44029304
0.1	0.5	0.04	0.1	0.2	0.1	2	-0.30961321	0.54080633
0.1	0.5	0.04	0.1	0.2	0.1	2.5	-0.31913355	0.62636326
0.1	0.5	0.04	0.1	0.2	0.1	3	-0.32608624	0.70165325

- The nonlinear mixed convection parameter affects the velocity field in a non-uniform way. It hurries the fluid motion in the region close to the plate wall, but it reduces the velocity away from the plate. In addition, it causes a decline in the thermal BLT and an enhancement in convective heat transfer compared with the linear mixed convection case.

- Both temperature-dependent and space-dependent heat sources increase the fluid temperature, thicken the thermal boundary layer, and reduce the wall heat transfer rate, whereas the corresponding heat sinks effectively enhance surface cooling by promoting heat removal from the fluid.
- The temperature-dependent and space-dependent heat source/sink parameters exhibit similar qualitative effects on the thermal field, indicating that both mechanisms are equally effective in controlling the thermal transport within the boundary layer.
- Increasing the velocity slip parameter weakens the momentum transfer from the wall to the fluid, resulting in lower wall shear stress, higher fluid temperature, and a larger thermal BLT.
- Thermal slip (temperature jump) reduces the amount of heat transferred from the surface to the fluid, thereby lowering both the fluid temperature and the fluid velocity while suppressing the development of the thermal boundary layer.
- The magnitude of the skin-friction coefficient declines with increasing assisting and nonlinear mixed convection parameters, heat source strength, and velocity slip, whereas it rises under opposing convection, heat sink conditions, and higher thermal slip.
- The local Nusselt number upsurges under assisting and nonlinear mixed convection as well as heat sink conditions, while it decays in the presence of heat sources and both velocity and thermal slips due to the reduction in the wall temperature gradient.

The present investigation focuses on nonlinear mixed convection over a vertically moving surface in the presence of temperature-dependent and space-dependent heat source/sink under partial slip boundary conditions. The current model can be extended to explore a wider range of practical thermal engineering applications by incorporating electrically conducting nanofluids or hybrid nanofluids in the presence of magnetic (MHD) effects, which provide additional mechanisms for controlling fluid motion and heat transfer. Furthermore, the analysis may be generalized by considering alternative boundary conditions, such as convective heating, variable wall temperature or variable heat flux, wall permeability, and nonlinear slip models, to better represent realistic industrial and technological processes.

Acknowledgments

The authors would like to express their sincere gratitude to the esteemed reviewers for their valuable comments and constructive suggestions, which have significantly improved the quality of the manuscript.

Funding

None.

Conflict of interest

There is no conflict of interest to disclose.

Author contributions

All authors contributed equally to this work and approved the final version of the manuscript.

Declaration of using AI tools

The authors declare that they have not used any type of generative artificial intelligence for the writing of this manuscript, nor for the creation of images, graphics, tables, or their corresponding captions.

References

[1] H. Blasius, “Grenzschichten in Flüssigkeiten mit kleiner Reibung,” *Z. Math. Phys.*, vol. 56, pp. 1-37, 1908.

[2] B. C. Sakiadis, “Boundary-layer behaviour on continuous solid surfaces: boundary-layer equations for two dimensional and axisymmetric flow,” *AIChE J.*, vol. 7, pp. 26-28, 1961.

[3] E. Pohlhausen, “Der Wärmeaustausch zwischen festen Körpern und Flüssigkeiten mit kleiner Reibung und kleiner Wärmeleitung,” *Z. Angew. Math. Mech.*, vol. 1, pp. 121-151, 1921.

[4] F.K. Tsou, E.M. Sparrow, and R.J. Goldstein, “Flow and heat transfer in the boundary layer on a continuous moving surface,” *Int. J. Heat Mass Transf.*, vol. 10, pp. 219-235, 1967.

[5] T. A. Abdelhafez, “Skin friction and heat transfer on a continuous flat surface moving in a parallel free stream,” *Int. J. Heat Mass Transf.*, vol. 28, pp. 1234-1237, 1985.

[6] N. Afzal, A. Badaruddin, and A. A. Elgarvi, “Momentum and heat transport on a continuous flat surface moving in a parallel stream,” *Int. J. Heat Mass Transf.*, vol. 36, no. 13, pp. 3399-3403, 1993.

[7] A. Ishak, “Radiation effects on the flow and heat transfer over a moving plate in a parallel stream,” Chin. Phys. Lett., vol. 26, no. 3, art. id 034701, 2009.

[8] S. Mukhopadhyay, K. Bhattacharyya, and G. C. Layek, "Steady boundary layer flow and heat transfer over a porous moving plate in presence of thermal radiation," *Int. J. Heat Mass Transf.*, vol. 54, no. 13-14, pp. 2751-2757, 2011.

[9] S. Dholey, "On the fluid dynamics of unsteady separated stagnation-point flow of a power-law fluid on the surface of a moving flat plate," *Eur. J. Mech. B Fluids*, vol. 70, pp. 102-114, 2018.

[10] A. Renuka, M. Muthtamilselvan, Q. M. Al-Mdallal, D. H. Doh, and B. Abdalla, "Unsteady Separated Stagnation Point Flow of Nanofluid past a Moving Flat Surface in the Presence of Buongiorno's Model," J. Appl. Comput. Mech., vol. 7, no. 3, pp. 1283-1290, 2021.

[11] N. S. Khashi'ie, N. M. Arifin, and I. Pop, "Magnetohydrodynamics (MHD) boundary layer flow of hybrid nanofluid over a moving plate with Joule heating," *Alex. Eng. J.*, vol. 61, no. 3, pp. 1938-1945, 2022.

[12] B. Gebhart, Y. Jaluria, R.L. Mahajan, and B. Sammakia, *Buoyancy Induced Flows and Transport*, New York, Hemisphere, 1988.

[13] N. Afzal, and T. Hussain, "Mixed convection over a horizontal plate," *J. Heat Transf.*, vol. 106, pp. 240-241, 1986.

[14] A. Hamid, M. Alghamdi, M. Khan, and A. S. Alshomrani, "An investigation of thermal and solutal stratification effects on mixed convection flow and heat transfer of Williamson nanofluid," *J. Mol. Liq.*, vol. 284, pp. 307-315, 2019.

[15] A. Abbas, M. Ashraf, and A.J. Chamkha, "Combined effects of thermal radiation and thermophoretic motion on mixed convection boundary layer flow," *Alex. Eng. J.*, vol. 60, no. 3, pp. 3243-3252, 2021.

[16] N. S. Wahid, N. M. Arifin, N. S. Khashi'ie, I. Pop, N. Bachok, and M. E. Hafidzuddin, "MHD mixed convection flow of a hybrid nanofluid past a permeable vertical flat plate with thermal radiation effect," *Alex. Eng. J.*, vol. 61, no. 4, pp. 3323-3333, 2022.

[17] S. L. Goren, "On free convection in water at 4°C," *Chem. Eng. Sci.*, vol. 21, no 6-7, pp. 515-518, 1966.

[18] M. Bandaru, M. M. Rashidi, and H. S. Raju, "Influence of non-linear convection and thermophoresis on heat and mass transfer from a rotating cone to fluid flow in porous medium," *Ther. Sci.*, vol. 21, no. 6 Part B, pp. 2781-2793, 2017.

[19] A. Alsaedi, T. Hayat, S. Qayyum, and R. Yaqoob, "Eyring–Powell nanofluid flow with nonlinear mixed convection: entropy generation minimization," *Comput. Methods Programs Biomed.*, vol. 186, pp. 105183, 2020.

[20] P. M. Patil, and M. Kulkarni, "Nonlinear mixed convective nanofluid flow along moving vertical rough plate," *Revista mexicana de fisica.*, vol. 66, no. 2, pp. 153-161, 2020.

[21] P. M. Patil, M. Kulkarni, and P. S. Hiremath, "Nonlinear mixed convection flow of nanofluid past a moving vertical slender cylinder," *Arab. J. Sci. Eng.*, vol. 45, no. 2, pp. 1219-1228, 2020.

[22] S. Rajput, V. K. Verma, K. Bhattacharyya, and A. J. Chamkha, "Unsteady nonlinear mixed convective flow of nanofluid over a wedge: Buongiorno model," *Waves Random Complex Media*, 2021, DOI: 10.1080/17455030.2021.1987586.

[23] S. Mukhopadhyay, "Heat transfer analysis of the unsteady flow of a Maxwell fluid over a stretching surface in the presence of a heat source/sink," *Chin. Phys. Lett.*, vol. 29, no. 5, art. id. 054703, 2012.

[24] B. J. Gireesha, K. G. Kumar, G. K. Ramesh, and B. C. Prasannakumara, "Nonlinear convective heat and mass transfer of Oldroyd-B nanofluid over a stretching sheet in the presence of uniform heat source/sink," Results Phys., 2018;9:1555-63.

[25] N. C. Roy, and I. Pop, "Dual solutions of magnetohydrodynamic mixed convection flow of an Oldroyd-B nanofluid over a shrinking sheet with heat source/sink," *Alex. Eng. J.*, vol. 61, no. 8, pp. 5939-5948, 2022.

[26] M. S. Abel, and N. Mahesha, "Heat transfer in MHD viscoelastic fluid flow over a stretching sheet with variable thermal conductivity, non-uniform heat source and radiation," *Appl. Math. Model.*, vol. 32, no. 10, pp. 1965-1983, 2008.

[27] D. Mythili, and R. Sivaraj, "Influence of higher order chemical reaction and non-uniform heat source/sink on Casson fluid flow over a vertical cone and flat plate," *J. Mol. Liq.*, vol. 216, pp. 466-475, 2016.

[28] B. J. Gireesha, B. Mahanthesh, R. S. Gorla, and K. L. Krupalakshmi, "Mixed convection two-phase flow of Maxwell fluid under the influence of non-linear thermal radiation, non-uniform heat source/sink and fluid-particle suspension," *Ain Shams Eng. J.*, vol. 9, no. 4, pp. 735-746, 2018.

[29] U. Khan, A. Zaib, A. Ishak, E. S. Sherif, I. Waini, Y. M. Chu, and I. Pop, "Radiative mixed convective flow induced by hybrid nanofluid over a porous vertical cylinder in a porous media with irregular heat sink/source," *Case Stud. Therm. Eng.*, vol. 30, art. id. 101711, 2022.

[30] M. Gad-el-Hak, "The Fluid Mechanics of Microdevices – The Freeman Scholar Lecture," J. Fluids Eng., vol. 121, art. id. 5, 1999.

[31] C. L. M. H. Navier, "Memoire Surles du Movement des," *Mémoires de l'Académie Royale des Sciences de l'Institut de France*, vol. 1, no. 6, pp. 414-416, 1823.

[32] S. Shah, and S. Hussain, "Slip effect on mixed convective flow and heat transfer of magnetized UCM fluid through a porous medium in consequence of novel heat flux model," *Results Phys.*, vol. 20, art. id. 103749, 2021.

[33] A. Haritha, Y. Devasena, and B. Vishali, "MHD heat and mass transfer of the unsteady flow of a Maxwell fluid over a stretching surface with Navier slip and convective boundary conditions," *Global J. Pure Appl. Math.*, vol. 13, no. 6, pp. 2169-2179, 2017.

[34] W. Ibrahim, and M. Negera, "MHD slip flow of upper-convected Maxwell nanofluid over a stretching sheet with chemical reaction," *J. Egypt. Math. Soc*., vol. 7, pp. 1-28, 2020.

[35] H. Waqas, M. Imran, S. Khan, S. A. Shehzad, and M. A. Meraj, "Slip flow of Maxwell viscoelasticity-based micropolar nanoparticles with porous medium: a numerical study," *Appl. Math. Mech. (Engl. Ed.*), vol. 40, pp. 1255-1268, 2019.

[36] J. Li, L. Zheng, and L. Liu, "MHD viscoelastic flow and heat transfer over a vertical stretching sheet with Cattaneo-Christov heat flux effects," *J. Mol. Liq.*, vol. 221, pp. 19-25, 2016.

[37] I. Uddin, R. Akhtar, M. A. R. Khan, Z. Zhiyu, S. Islam, M. Shoaib, and M. A. Z. Raja, "Numerical treatment for fluidic system of activation energy with non-linear mixed convective and radiative flow of magneto nanomaterials with Navier's velocity slip," AIP Adv., vol. 9, art. id. 055210, 2019.

[38] R. C. Bataller, "Numerical comparisons of Blasius and Sakiadis flows," Matematika, vol. 26, pp. 187-196, 2010.

[39] S. Ahmad, A. M. Rohni, and I. Pop, "Blasius and Sakiadis problems in nanofluids," Acta Mechanica, vol. 218, pp. 195-204, 2011.

[40] N. H. A. Rahman, N. Bachok, and H. Rosali, "Boundary-layer flow and heat transfer of blasius and sakiadis problems in nanofluids with partial slip and thermal convection," CFD Letters, vol. 11, pp. 53-65, 2019.

All open access articles published in Transactions on Computational Modeling and Intelligent Systems (http://tcmis.org) are distributed under the terms of the CC BY-NC 4.0 license (Creative Commons Attribution Non-Commercial 4.0 International Public License as currently displayed at http://creativecommons.org/licenses/by-nc/4.0/legalcode) which permits unrestricted use, distribution, and reproduction in any medium, for non-commercial purposes, provided the original work is properly cited.